PHYSICAL REVIEW D **94,** 015021 (2016)

Production and decay of the diphoton resonance at future e^+e^- colliders

Hayato Ito and Takeo Moroi
Department of Physics, University of Tokyo, Tokyo 113-0033, Japan
(Received 19 April 2016; published 18 July 2016)

Motivated by the ATLAS and CMS announcements of the excesses of diphoton events, we discuss the production and decay processes of diphoton resonance at future e^+e^- colliders. We assume that the excess of the diphoton events at the LHC is explained by a scalar resonance decaying into a pair of photons. In such a case, the scalar interacts with standard model gauge bosons and, consequently, the production of such a scalar is possible at the e^+e^- colliders. We study the production of the scalar resonance via the associated production with the photon or Z, as well as via the vector-boson fusion, and calculate the cross sections of these processes. We also study the backgrounds, and discuss the detectability of the signals of scalar production with various decay processes of the scalar resonance. We also consider the case where the scalar resonance has an invisible decay mode, and study how the invisible decay can be observed at the e^+e^- colliders.

DOI: 10.1103/PhysRevD.94.015021

I. INTRODUCTION

High energy e^+e^- linear colliders, like THE International e^+e^- Linear Collider (ILC) [1–5] and Compact Linear Collider (CLIC) [6], are attractive candidates of energy frontier experiments in the future. The future e^+e^- colliders will not only study the detail of standard model (SM) particles, particularly Higgs boson and top quark, but also provide important information about new physics at the electroweak scale (if it exists). For the e^+e^- linear collider experiments in the future, it is crucial to understand how and how well the information about various new physics models can be obtained there.

Notably, in December of 2015, both the ATLAS and CMS Collaborations announced the excess in the diphoton invariant mass distribution [7,8]. The ATLAS Collaboration observed the excess with 3.6-σ (2.0-σ) local (global) significance at $M_{\gamma\gamma} \simeq 750$ GeV (with $M_{\gamma\gamma}$ being the diphoton invariant mass) for a narrow width case. Furthermore, the CMS Collaboration result shows an excess with the local (global) significance of 2.6-σ (1.2-σ) at $M_{\gamma\gamma} \simeq 760$ GeV. These signals may indicate the existence of a new scalar resonance with the mass of $\sim$750 GeV, although more data is needed to confirm or exclude such a possibility (see, for example, [9–19]). If there exists such a resonance, its properties should be studied in detail by the future e^+e^- collider experiments [20–23].

Currently, the ILC is planning to be extendable up to $\sqrt{s} \sim 1$ TeV [with $\sqrt{s}$ being the center-of-mass (CM) energy of the collider]. In addition, the energy of CLIC can be as high as a few TeV. With such CM energies, the resonance with its mass of $\sim$750 GeV is kinematically reachable. In particular, in some class of models, the resonance can be produced in association with neutral electroweak gauge bosons (i.e., γ or Z) and via the vector-boson fusion processes at the e^+e^- colliders. Once produced, the properties of the resonance may be studied with a high luminosity and a clean environment of the future e^+e^- colliders.

If there exists a new resonance, it is important to understand how it interacts with other fields. As mentioned above, one attractive explanation of the LHC diphoton excess is the existence of a scalar resonance with its mass of $\sim$750 GeV coupled to the SM gauge bosons. In addition, as well as the coupling to the gauge bosons, the scalar boson may also couple to other fields. For example, the scalar resonance may have a coupling to an invisible new particle which may be dark matter of the Universe (see, for example, [10,11]). An understanding of the properties of the scalar resonance will be a very important issue if it exists.

The purpose of this paper is to consider the production and the decay of the scalar boson (which we call Φ), which is responsible for the LHC diphoton excess, at the future e^+e^- colliders. We calculate the production cross section of such a scalar resonance at the e^+e^- colliders. We also estimate the number of backgrounds, and discuss the detectability of each decay mode of Φ.

The organization of this paper is as follows. In Sec. II, we summarize the model we consider. In Sec. III, we discuss the production processes of Φ at the e^+e^- colliders. In particular, we study the production of Φ in association with γ or Z, and also the production via the vector-boson fusion processes. In Sec. IV, we consider the detectability of the Φ production signal in which Φ decays into SM gauge bosons. The detectability of the invisible decay of Φ is discussed in Sec. V. Section VI is devoted for conclusions and discussion.

II. MODEL

Let us first summarize the interaction of the new scalar boson of our interest. In order to make our discussion

concrete, we assume that the scalar boson Φ is pseudoscalar, and that it has the following interaction:

$$\mathcal{L}_{\rm eff} = \frac{1}{2\Lambda_1}\Phi\epsilon^{\mu\nu\rho\sigma}\mathcal{B}_{\mu\nu}\mathcal{B}_{\rho\sigma} + \frac{1}{2\Lambda_2}\Phi\epsilon^{\mu\nu\rho\sigma}\mathcal{W}^a_{\mu\nu}\mathcal{W}^a_{\rho\sigma} + \frac{1}{2\Lambda_3}\Phi\epsilon^{\mu\nu\rho\sigma}\mathcal{G}^A_{\mu\nu}\mathcal{G}^A_{\rho\sigma}, \tag{2.1}$$

where $\mathcal{B}_{\mu\nu}$, $\mathcal{W}^a_{\mu\nu}$, and $\mathcal{G}^A_{\mu\nu}$ are field strength tensors for $U(1)_Y$, $SU(2)_L$, and $SU(3)_C$ gauge interactions, respectively, and the superscripts a and A are indices of the adjoint representations of $SU(2)_L$ and $SU(3)_C$, respectively. (Even if Φ is a real scalar boson, the following results are almost unchanged.) The summations over the repeated indices are implicit. Because the interactions given in Eq. (2.1) are nonrenormalizable, it is expected that there exists some dynamics which generates the interaction between Φ and SM gauge bosons. We do not specify the dynamics behind the effective Lagrangian, and use Eq. (2.1) for our study.[1]

With the above interaction terms, the partial decay rates of Φ into the gauge bosons are given by

$$\Gamma(\Phi \to gg) = \frac{2m_\Phi^3}{\pi\Lambda_3^2}, \tag{2.2}$$

$$\Gamma(\Phi \to \gamma\gamma) = \frac{m_\Phi^3}{4\pi\Lambda_{\gamma\gamma}^2}, \tag{2.3}$$

$$\Gamma(\Phi \to \gamma Z) = \frac{m_\Phi^3}{8\pi\Lambda_{\gamma Z}^2}\left(1-\frac{m_Z^2}{m_\Phi^2}\right)^3, \tag{2.4}$$

$$\Gamma(\Phi \to ZZ) = \frac{m_\Phi^3}{4\pi\Lambda_{ZZ}^2}\left(1-\frac{4m_Z^2}{m_\Phi^2}\right)^{3/2}, \tag{2.5}$$

$$\Gamma(\Phi \to W^+W^-) = \frac{m_\Phi^3}{2\pi\Lambda_2^2}\left(1-\frac{4m_W^2}{m_\Phi^2}\right)^{3/2}, \tag{2.6}$$

where m_Φ, m_Z, and m_W are the masses of Φ, Z, and $W^\pm$, respectively. For the definitions of $\Lambda_{\gamma\gamma}$, $\Lambda_{\gamma Z}$, and Λ_{ZZ}, see the Appendix. As we have mentioned, we also consider the case where Φ has an invisible decay mode. In such a case, we treat the invisible decay width $\Gamma(\Phi \to \chi\chi)$ as a free parameter without specifying the interaction giving rise to such a decay. (Here and hereafter, the invisible particle is denoted as χ.) One example is the interaction of the form of $\Phi\chi\chi$, with which χ is regarded as a gauge singlet Weyl fermion. For the total decay width Γ_Φ, because Φ may decay into particles other than the SM gauge bosons or the invisible particle, Γ_Φ is regarded as a free parameter. In addition, we assume that $\Gamma_\Phi \ll m_\Phi$ so that the narrow width approximation is applicable.

In the following, we consider two possible production processes at the LHC. One is the gluon-gluon fusion process, for which the LHC cross section (with the CM energy of 13 TeV) is estimated as

$$\sigma^{(gg)}_{\rm LHC}(pp \to \Phi \to \gamma\gamma) \simeq 6.6\ {\rm fb} \times \frac{\Gamma(\Phi \to gg)}{\Gamma_\Phi} \times \left[\frac{\Gamma(\Phi \to \gamma\gamma)}{1\ {\rm MeV}}\right], \tag{2.7}$$

and the other is photon-photon fusion process [24,25], for which

$$\sigma^{(\gamma\gamma)}_{\rm LHC}(pp \to \Phi \to \gamma\gamma) \simeq 24\ {\rm fb} \times \left[\frac{\Gamma_\Phi}{100\ {\rm MeV}}\right]^{-1} \times \left[\frac{\Gamma(\Phi \to \gamma\gamma)}{100\ {\rm MeV}}\right]^2. \tag{2.8}$$

One should note that, with the diphoton production cross section at the LHC being fixed, a larger value of $\Gamma(\Phi \to \gamma\gamma)$ is needed for the case of photon-photon fusion dominance compared to the gluon-gluon fusion dominance. This fact has an important implication to the e^+e^- colliders.

III. PRODUCTION OF Φ AT THE e^+e^- COLLIDERS

With the interaction given in Eq. (2.1), the Φ production may occur at the e^+e^- colliders via several processes. We first consider the production processes in association with neutral electroweak gauge bosons:

(i) $e^+e^- \to \Phi\gamma$,
(ii) $e^+e^- \to \Phi Z$.

Feynman diagrams contributing to these processes are shown in Fig. 1. The analytic expressions of the cross sections of these processes are given in the Appendix. In order to discuss the production process of Φ at the e^+e^- colliders in light of the LHC diphoton excess, it is convenient to parametrize the cross sections of these processes by using the LHC cross sections. Notably, the ratio $\sigma(e^+e^- \to \Phi V)/\Gamma(\Phi \to \gamma\gamma)$ depends only on the ratio Λ_1/Λ_2 (where $V = \gamma$ or Z). Then, using Eq. (2.7), one can see that the following relation holds:

$$\sigma(e^+e^- \to \Phi V){\rm Br}(\Phi \to F) \simeq \bar{\sigma}^{(gg)}_{\Phi V} \times \frac{\Gamma(\Phi \to F)}{\Gamma(\Phi \to gg)} \times \left[\frac{\sigma^{(gg)}_{\rm LHC}(pp \to \Phi \to \gamma\gamma)}{10\ {\rm fb}}\right], \tag{3.1}$$

[1] If the energy of the collider becomes larger than the energy scale of the new physics responsible for the effective interaction, the calculation based on Eq. (2.1) may be inaccurate. We assume that it is not the case. In particular, if the scale of generating $\mathcal{L}_{\rm eff}$ is close to $\sim\frac{1}{2}\sqrt{s}$, on the contrary, momentum-dependent corrections to the effective Lagrangian can become sizable. The study of such an effect is interesting because it may reveal the dynamics behind the interaction of Φ with the SM gauge bosons. Such an issue is, however, beyond the scope of our study, and we leave it for future study.

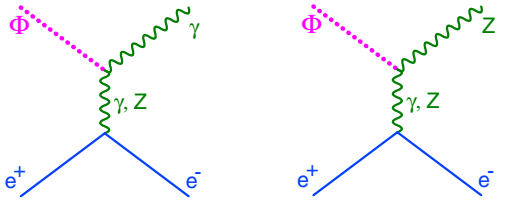

FIG. 1. The Feynman diagrams for the processes $e^+e^- \to \Phi\gamma$ and ΦZ.

where $\bar{\sigma}^{(V)}_{gg}$ depends only on the ratio Λ_1/Λ_2 (as far as m_Φ and $\sqrt{s}$ are fixed). The above relation is useful when the LHC diphoton excess originates from the gluon-gluon fusion. In addition, using Eq. (2.8), we define $\bar{\sigma}^{(\gamma\gamma)}_{\Phi V}$, which is also a function of Λ_1/Λ_2, as

$$\sigma(e^+e^- \to \Phi V)\mathrm{Br}(\Phi \to F) \simeq \bar{\sigma}^{(\gamma\gamma)}_{\Phi V} \times \frac{\Gamma(\Phi \to F)}{\Gamma(\Phi \to \gamma\gamma)} \times \left[\frac{\sigma^{(\gamma\gamma)}_{\mathrm{LHC}}(pp \to \Phi \to \gamma\gamma)}{10\ \mathrm{fb}}\right]. \quad (3.2)$$

This expression can be used when the photon-photon fusion process is important at the LHC.

In Figs. 2 and 3, we plot $\bar{\sigma}^{(gg)}_{\Phi\gamma}$ and $\bar{\sigma}^{(gg)}_{\Phi Z}$ as functions of Λ_1/Λ_2, taking $\sqrt{s} = 1$, 1.5, 2, and 3 TeV.[2] (Here and hereafter, we take $m_\Phi = 750$ GeV for our numerical calculations.) Here, the electron and positron beams are unpolarized, i.e., $P_{e^-} = P_{e^+} = 0$ (with P_{e^-} and P_{e^+} being the mean helicities of the initial-state electron and positron, respectively). Notice that the regions with too small or too large Λ_1/Λ_2 are excluded by the 8 TeV run of the LHC. The most stringent bound comes from the negative searches for the resonance which decays into γZ; for example, taking $\sigma(pp \to \Phi \to \gamma Z; 8\ \mathrm{TeV}) < 11$ fb [17,26] and the LHC cross section of the diphoton signal events to be 10 fb, only the region with $-1 \lesssim \Lambda_1/\Lambda_2 \lesssim 6$ is allowed. In such a region, $\bar{\sigma}^{(gg)}_{\Phi\gamma}$ and $\bar{\sigma}^{(gg)}_{\Phi Z}$ are both of $O(10^{-2}$ fb) or smaller with $\sqrt{s} = 1$ TeV. With larger CM energy of ∼1.5–2 TeV, the cross sections may be as large as ∼0.1 fb. In addition, in order to see how the cross sections depend on the beam polarizations, we also show $\bar{\sigma}^{(gg)}_{\Phi\gamma}$ and $\bar{\sigma}^{(gg)}_{\Phi Z}$ for $P_{e^-} = \pm 0.8$ and $P_{e^+} = \mp 0.3$ in Figs. 4 and 5, respectively, taking $\sqrt{s} = 1$ TeV.

Next, we consider the processes:

(i) $e^+e^- \to \Phi e^+e^-$,

(ii) $e^+e^- \to \Phi\bar{\nu}_e\nu_e$,

to which the vector-boson fusion diagrams contribute (see Fig. 6). For these processes, we define

[2]Here and hereafter, the effect of the initial-state radiation is neglected.

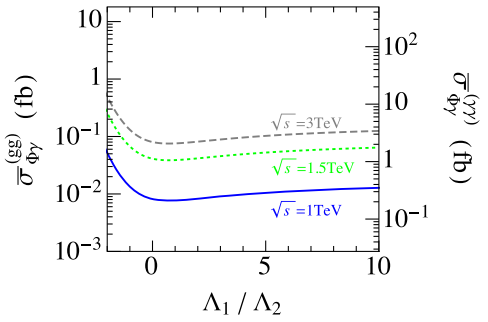

FIG. 2. $\bar{\sigma}^{(gg)}_{\Phi\gamma}$ as a function of Λ_1/Λ_2, with $\sqrt{s} = 1$, 1.5, and 3 TeV. Here we take $P_{e^-} = P_{e^+} = 0$. The right-horizontal axis shows the value of $\bar{\sigma}^{(\gamma\gamma)}_{\Phi\gamma}$ using Eq. (3.9).

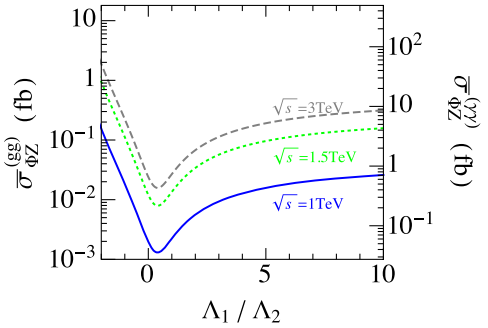

FIG. 3. $\bar{\sigma}^{(gg)}_{\Phi Z}$ as a function of Λ_1/Λ_2, with $\sqrt{s} = 1$, 1.5, and 3 TeV. Here we take $P_{e^-} = P_{e^+} = 0$. The right-horizontal axis shows the value of $\bar{\sigma}^{(\gamma\gamma)}_{\Phi Z}$ using Eq. (3.9).

$$\sigma(e^+e^- \to \Phi\bar{l}l)\mathrm{Br}(\Phi \to F) \simeq \bar{\sigma}^{(gg)}_{\Phi\bar{l}l} \times \frac{\Gamma(\Phi \to F)}{\Gamma(\Phi \to gg)} \times \left[\frac{\sigma^{(gg)}_{\mathrm{LHC}}(pp \to \Phi \to \gamma\gamma)}{10\ \mathrm{fb}}\right], \quad (3.3)$$

and

$$\sigma(e^+e^- \to \Phi\bar{l}l)\mathrm{Br}(\Phi \to F) \simeq \bar{\sigma}^{(\gamma\gamma)}_{\Phi\bar{l}l} \times \frac{\Gamma(\Phi \to F)}{\Gamma(\Phi \to \gamma\gamma)} \times \left[\frac{\sigma^{(\gamma\gamma)}_{\mathrm{LHC}}(pp \to \Phi \to \gamma\gamma)}{10\ \mathrm{fb}}\right], \quad (3.4)$$

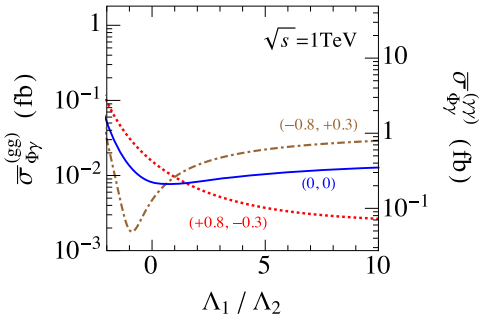

FIG. 4. $\bar{\sigma}^{(gg)}_{\Phi\gamma}$ as a function of Λ_1/Λ_2, with $\sqrt{s} = 1$ TeV, taking $(P_{e^-}, P_{e^+}) = (+0.8, -0.3)$ (red dashed), $(-0.8, +0.3)$ (brown dot-dashed), and (0,0) (blue solid). The right-horizontal axis shows the value of $\bar{\sigma}^{(\gamma\gamma)}_{\Phi\gamma}$ using Eq. (3.9).

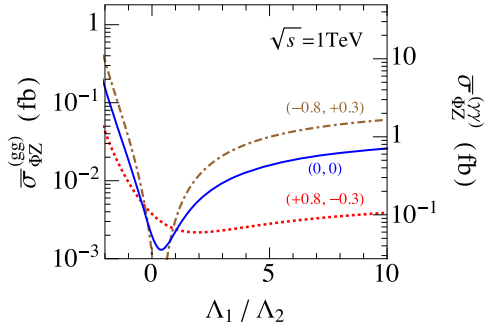

FIG. 5. $\bar{\sigma}^{(gg)}_{\Phi Z}$ as a function of Λ_1/Λ_2, with $\sqrt{s} = 1$ TeV, taking $(P_{e-}, P_{e+}) = (+0.8, -0.3)$ (red dashed), $(-0.8, +0.3)$ (brown dot-dashed), and (0,0) (blue solid). The right-horizontal axis shows the value of $\bar{\sigma}^{(\gamma\gamma)}_{\Phi\gamma}$ using Eq. (3.9).

with $\bar{l}l = e^+e^-$ or $\bar{\nu}_e\nu_e$. Then, $\bar{\sigma}^{(gg)}_{\Phi\bar{l}l}$ and $\bar{\sigma}^{(\gamma\gamma)}_{\Phi\bar{l}l}$ depend only on Λ_1/Λ_2.

The cross section of the process $e^+e^- \to \Phi e^+e^-$ is enhanced when the scattering angles of final-state e^+ and e^- are both small. In such a case, the photon-photon fusion diagram shown in Fig. 6 is enhanced because the virtual photons are almost on shell so that the denominators of the photon propagators become extremely small. Then, the photon-photon fusion diagram dominates over other diagrams which are less singular. In order to treat such an effect properly, we use the equivalent photon approximation [27]. For simplicity, we concentrate on the case with unpolarized electron and positron beams. Then, for the case where the scattering angles of electron and positron are both small enough, we can approximate

$$\sigma(e^+e^- \to Fe^+e^-) \simeq \int dx dx' f_\gamma(x; \theta^{(\min)}_{e^+}, \theta^{(\max)}_{e^+}) \times f_\gamma(x'; \theta^{(\min)}_{e^-}, \theta^{(\max)}_{e^-}) \sigma(\gamma\gamma \to F; sxx'), \tag{3.5}$$

where $\theta^{(\min)}_{e^\pm}$ and $\theta^{(\max)}_{e^\pm}$ are minimal and maximal scattering angles of $e^\pm$, respectively, and $\sigma(\gamma\gamma \to F; E^2_{\rm cm})$ is the cross section of the unpolarized photon-photon collision process $\gamma\gamma \to F$ with the center-of-mass energy $E_{\rm cm}$. In addition, f_γ is the distribution function of the photon; for $0 < x < 1$, f_γ is given by

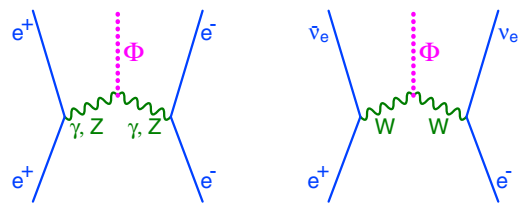

FIG. 6. The vector-boson fusion diagrams contributing to the Φ productions.

$$f_\gamma(x, \theta^{(\min)}, \theta^{(\max)}) = \frac{\alpha}{2\pi}\left[\frac{1+(1-x)^2}{x}\ln\frac{|q^2|^{(\max)}}{|q^2|^{(\min)}} - 2m_e^2 x\frac{|q^2|^{(\max)} - |q^2|^{(\min)}}{|q^2|^{(\max)}|q^2|^{(\min)}}\right], \tag{3.6}$$

with m_e being the electron mass, and

$$|q^2|^{(\min,\max)} \equiv \frac{1}{2}s(1-x)\left[1 - \cos\theta^{(\min,\max)} + \frac{2x^2}{(1-x)^2}\frac{m_e^2}{s}\right], \tag{3.7}$$

while, otherwise, $f_\gamma = 0$. For the process of our interest, we obtain

$$\sigma(e^+e^- \to \Phi e^+e^-) \simeq \frac{8\pi^2\Gamma(\Phi \to \gamma\gamma)}{sm_\Phi}\int\frac{dx}{x} \times f_\gamma(x; \theta^{(\min)}_{e^+}, \theta^{(\max)}_{e^+}) \times f_\gamma(m_\Phi^2/sx; \theta^{(\min)}_{e^-}, \theta^{(\max)}_{e^-}), \tag{3.8}$$

where we used narrow width approximation.

The cross section of the process $e^+e^- \to \Phi e^+e^-$ is logarithmically enhanced when $\theta^{(\min)}_{e^\pm} \ll 1$. For the study of the process $e^+e^- \to \Phi e^+e^-$, the energetic $e^\pm$ in the forward direction may be used to eliminate the backgrounds. Since the ILC forward detectors are expected to cover up to $O(1$–$10)$ mrad [5], we assume that energetic $e^\pm$ with its energy $E_{e^\pm}$ larger than 50 GeV can be identified with significant efficiency if the scattering angle $\theta_{e^\pm}$ is larger than 10 mrad. We calculate the cross section, requiring that e^+ and e^- are emitted to the forward directions. We consider the following three different requirements:

(i) Requirement 0: There is no $e^\pm$ with $\theta_{e^\pm} > 100$ mrad. (In this case, the scattering angles of $e^\pm$ may be both so small that neither of $e^\pm$ are detected.)
(ii) Requirement 1: There is at least one $e^\pm$ with $E_{e^\pm} > 50$ GeV and $\theta_{e^\pm} > 10$ mrad. In addition, $\theta_{e^\pm} < 100$ mrad is required for both e^+ and e^-.
(iii) Requirement 2: The energies and the scattering angles of both e^+ and e^- satisfy $E_{e^\pm} > 50$ GeV and $10 < \theta_{e^\pm} < 100$ mrad.

The results are shown in Table I. (Notice that with the equivalent photon approximation, $\bar{\sigma}^{(gg)}_{\Phi e^+e^-}$ is independent of Λ_1/Λ_2.) We have also checked that, if we require $\theta_{e^\pm} > 20$ mrad for the detection instead of 10 mrad, $\bar{\sigma}^{(gg)}_{\Phi e^+e^-}$ decreases by ∼30% and ∼50% for the cases of Requirements 1 and 2, respectively.

For the process $e^+e^- \to \Phi\bar{\nu}_e\nu_e$, the W-boson fusion diagram contributes. Even though W is massive, such a diagram is enhanced when the neutrinos are emitted to the forward directions in the high energy limit. We have also

TABLE I. $\bar{\sigma}^{(gg)}_{\Phi e^+e^-}$ for $\sqrt{s} = 1$, 1.5, 2, and 3 TeV, adopting the Requirements 0, 1 or 2. $\bar{\sigma}^{(\gamma\gamma)}_{\Phi e^+e^-}$ can be obtained by using Eq. (3.9).

$\sqrt{s}$	Requirement 0	Requirement 1	Requirement 2
1 TeV	0.044 fb	0.015 fb	0.002 fb
1.5 TeV	0.18 fb	0.065 fb	0.007 fb
2 TeV	0.35 fb	0.12 fb	0.012 fb
3 TeV	0.70 fb	0.22 fb	0.022 fb

calculated the cross section of such a process, and found that the cross section is $O(10^{-3}$ fb) or smaller for $\sqrt{s} = 1$ TeV, for example. Furthermore, because there is no activity other than the decay products of Φ in this process, we expect that the background reduction is much more difficult than the case of $e^+e^- \to \Phi e^+e^-$.

So far, we have studied $\bar{\sigma}^{(gg)}_{\Phi X}$ (with $X = \gamma$, Z, e^+e^-, or $\bar{\nu}_e\nu_e$). For the calculations of $\bar{\sigma}^{(\gamma\gamma)}_{\Phi X}$, we can use the following proportionality:

$$\bar{\sigma}^{(\gamma\gamma)}_{\Phi X} \simeq 27\bar{\sigma}^{(gg)}_{\Phi X}. \tag{3.9}$$

In particular, the values of $\bar{\sigma}^{(\gamma\gamma)}_{\Phi\gamma}$ and $\bar{\sigma}^{(\gamma\gamma)}_{\Phi Z}$ are also shown in Figs. 2 and 3, respectively. When the LHC diphoton excess at the LHC originates from the photon-photon fusion, the cross sections at the e^+e^- colliders become larger compared to the case of gluon-gluon fusion at the LHC. This is because, for the former case, a larger value of $\Gamma(\Phi \to \gamma\gamma)$ needed (with the diphoton cross section at the LHC being fixed), resulting in stronger interaction of Φ with electroweak gauge bosons.

IV. DECAY INTO SM GAUGE BOSONS

Now we are at the position to discuss the possibility of detecting the Φ production at the future e^+e^- colliders. In this section, we consider the decay of Φ into SM gauge bosons.

A. $e^+e^- \to \Phi\gamma$ and $e^+e^- \to \Phi Z$

We first consider the Φ production in association with a SM gauge boson, $e^+e^- \to \Phi V$, followed by $\Phi \to V_1' V_2'$, where $V = \gamma$ or Z, and $(V_1', V_2') = (g, g)$, (γ, γ), (γ, Z), (Z, Z), or (W^+, W^-). One characteristic feature of such an event is the existence of a monochromatic gauge boson. With the process $e^+e^- \to \Phi V$, the energy of the gauge boson V is given by

$$E_V^{(\mathrm{sig})} = \frac{s - m_\Phi^2 + m_V^2}{2\sqrt{s}}, \tag{4.1}$$

where m_V is the mass of V. For the processes $e^+e^- \to \Phi\gamma$ and ΦZ, $(E_\gamma^{(\mathrm{sig})}, E_Z^{(\mathrm{sig})}) = (219\ \mathrm{GeV}, 223\ \mathrm{GeV})$ [(859 GeV, 861 GeV), (1046 GeV, 1048 GeV)] for $\sqrt{s} = 1$ TeV (2 TeV, 3 TeV), respectively. The kinematical cut based on $E_V^{(\mathrm{sig})}$ can be used to reduce backgrounds.

To estimate the number of backgrounds, we calculate the SM cross sections to produce γ or Z whose energy is close to $E_V^{(\mathrm{sig})}$ in association with two other gauge bosons (or energetic jets). For simplicity, we do not consider the decay of weak bosons nor the hadronization of partons. Then, in studying the backgrounds for the signal of $e^+e^- \to \Phi\gamma$, the following kinematical requirement is imposed:

(i) There is one photon whose energy satisfies $|E_\gamma - E_\gamma^{(\mathrm{sig})}| < 0.02E_\gamma^{(\mathrm{sig})}$, where E_γ is the energy of photon.

For the backgrounds for $e^+e^- \to \Phi Z$, we require

(i) There is one Z whose energy satisfies $|E_Z - E_Z^{(\mathrm{sig})}| < 0.06E_Z^{(\mathrm{sig})}$, where E_Z is the energy of Z.

Notice that a very accurate measurement of the photon energy is expected at the ILC [5]; with the energy resolution of the electromagnetic calorimeter of the SiD detector, for example, $\delta E/E = 0.17/\sqrt{E} \oplus 1\%$ for electrons or photons. Furthermore, with the ILC detectors, the jet energy will be measured with the accuracy of 3% or better for jet energies above 100 GeV. Thus, we take ~2-σ width of the detector resolution, assuming that we use the hadronic decay mode of Z for the latter process. In addition, we require that all the activities satisfy

(i) $|\eta| < 3$,

where η is the pesudorapidity.

For the signal events in which Φ decays into a gluon pair, we expect that the dominant source of the backgrounds is $e^+e^- \to q\bar{q}V$, where q denotes light quarks; we calculate the SM cross sections of such processes with the cuts mentioned above. [In such a case, (V_1', V_2') should be understood as $(q, \bar{q})$.] For other cases, we calculate the SM cross section of the process $e^+e^- \to V_1' V_2' V$. The candidate of V (i.e., the gauge boson produced in association with Φ) is expected to be identified by using Eq. (4.1). In addition, we use the fact that the final states with $(V_1', V_2') = (Z, Z)$ and (W^+, W^-) can be distinguished with hadronically decaying Z and $W^\pm$, using the invariant masses of the decay products of V_1' and V_2' (which we denote $m_{V_1'}$ and $m_{V_2'}$, respectively) [5]. [In our study, we neglect the efficiency for the misidentification of $(V_1', V_2') = (Z, Z)$ and (W^+, W^-).] Assuming 3% uncertainty for the measurement of jet energies, the invariant masses of the Z and $W^\pm$ systems are expected to be determined with the accuracy of ~4 GeV, which is sizably smaller than the mass difference of Z and $W^\pm$. In particular, by studying $m_{V_1'}$ and $m_{V_2'}$ simultaneously, we expect that the $(V_1', V_2') = (Z, Z)$ and (W^+, W^-) final states are distinguishable.

The estimated numbers of backgrounds for the case of $\sqrt{s} = 1$, 2, and 3 TeV are summarized in Tables II, III, and IV, respectively.

TABLE II. The number of backgrounds for $e^+e^- \to \Phi\gamma$ and ΦZ, with $\sqrt{s} = 1$ TeV and $L = 1$ ab^{-1}. Here we take $P_{e^-} = P_{e^+} = 0$.

Signal	γgg	Zgg	$\gamma\gamma\gamma$	$\gamma\gamma Z$	γZZ	ZZZ	γW^+W^-	ZW^+W^-
$e^+e^- \to \Phi\gamma$	840	⋯	940	670	120	⋯	1200	⋯
$e^+e^- \to \Phi Z$	⋯	900	⋯	810	550	120	⋯	3000

TABLE III. Same as Table II, except for $\sqrt{s} = 2$ TeV.

Signal	γgg	Zgg	$\gamma\gamma\gamma$	$\gamma\gamma Z$	γZZ	ZZZ	γW^+W^-	ZW^+W^-
$e^+e^- \to \Phi\gamma$	510	⋯	1500	890	130	⋯	1800	⋯
$e^+e^- \to \Phi Z$	⋯	700	⋯	1800	1100	160	⋯	3800

TABLE IV. Same as Table II, except for $\sqrt{s} = 3$ TeV.

Signal	γgg	Zgg	$\gamma\gamma\gamma$	$\gamma\gamma Z$	γZZ	ZZZ	γW^+W^-	ZW^+W^-
$e^+e^- \to \Phi\gamma$	480	⋯	1900	1100	140	⋯	2400	⋯
$e^+e^- \to \Phi Z$	⋯	550	⋯	1900	1200	170	⋯	5000

To discuss the detectability of each mode, we define

$$S_{VV_1'V_2'}/\sqrt{B_{VV_1'V_2'}} \equiv \frac{L\sigma(e^+e^- \to \Phi V)\mathrm{Br}(\Phi \to V_1'V_2')\epsilon}{\sqrt{B_{VV_1'V_2'}}}, \tag{4.2}$$

where L is the luminosity, ϵ is the efficiency due to the rapidity cut, and $B_{VV_1'V_2'}$ is the number of backgrounds for the process $e^+e^- \to \Phi V$, followed by $\Phi \to V_1'V_2'$. Let us introduce

$$R_{\mathrm{EW}} \equiv \frac{\Gamma(\Phi\to\gamma\gamma)+\Gamma(\Phi\to\gamma Z)+\Gamma(\Phi\to ZZ)+\Gamma(\Phi\to W^+W^-)}{\Gamma(\Phi\to gg)}, \tag{4.3}$$

which parametrizes the ratio of the gluon-gluon fusion and photon-photon fusion contributions to the LHC diphoton events; with sufficiently small (large) value of R_{EW}, the LHC diphoton excess is explained by the gluon-gluon (photon-photon) fusion process. Then, the ratio $S_{VV_1'V_2'}/\sqrt{B_{VV_1'V_2'}}$ depends on the luminosity L, Λ_1/Λ_2, R_{EW}, and the LHC diphoton cross section $\sigma_{\mathrm{LHC}}(pp \to \Phi \to \gamma\gamma)$, where

$$\sigma_{\mathrm{LHC}}(pp \to \Phi \to \gamma\gamma) = \sigma^{(gg)}_{\mathrm{LHC}}(pp \to \Phi \to \gamma\gamma) + \sigma^{(\gamma\gamma)}_{\mathrm{LHC}}(pp \to \Phi \to \gamma\gamma). \tag{4.4}$$

For our numerical analysis, we take $\sigma_{\mathrm{LHC}}(pp \to \Phi \to \gamma\gamma) = 10\,\mathrm{fb}$. Using Eqs. (2.7) and (2.8), the gluon-gluon and photon-photon fusion contributions to the LHC diphoton cross section become comparable when $\Gamma(\Phi \to \gamma\gamma) \simeq 27\Gamma(\Phi \to gg)$.

First, let us consider the signal with $(V_1', V_2') = (g, g)$. The ratio $S_{Vgg}/\sqrt{B_{Vgg}}$ is maximized when the LHC diphoton excess is explained by the gluon-gluon fusion process. In such a case, $S_{Vgg}/\sqrt{B_{Vgg}}$ depends only on the ratio Λ_1/Λ_2; with $\sqrt{s} = 1$ TeV, it becomes larger than 5 when $-4.9 < \Lambda_1/\Lambda_2 < -2.5$ and $-8.2 < \Lambda_1/\Lambda_2 < -2.0$ for $V = \gamma$ and $V = Z$, respectively. With $\sigma_{\mathrm{LHC}}(pp \to \Phi \to \gamma\gamma) = 10$ fb, however, such a value of Λ_1/Λ_2 is already excluded by the 8 TeV run of the LHC, as we have mentioned in the previous section. Thus, with the Φ production in association with γ or Z, we expect that the detection of gg final state is difficult.

Next, we consider the other decay modes of Φ, i.e., $\Phi \to V_1'V_2'$ with $(V_1', V_2') = (\gamma, \gamma)$, (γ, Z), (Z, Z), or (W^+, W^-). As R_{EW} increases, the cross sections of the Φ production with such decay processes increase. We estimate the minimal value of R_{EW} to see the signals, requiring $S_{VV_1'V_2'}/\sqrt{B_{VV_1'V_2'}} > 5$. The results are shown in Figs. 7, 8, and 9 for $\sqrt{s} = 1$, 2, and 3 TeV, respectively. [In these figures, the integrated luminosity of $L = 1$ ab is used. For other values of the luminosity, the expected sensitivity is obtained by rescaling the results by $(L/1\ \mathrm{ab})^{-1/2}$.] In the figures, we shaded the region where $\sigma^{(\gamma\gamma)}_{\mathrm{LHC}}(pp \to \Phi \to \gamma\gamma)$ becomes larger than $\sigma^{(gg)}_{\mathrm{LHC}}(pp \to \Phi \to \gamma\gamma)$; thus, in the shaded region, the LHC diphoton excess is explained by the photon-photon fusion process. We can see that the detection and the study of Φ may be possible at the e^+e^- colliders with large enough R_{EW}. In particular, if the LHC diphoton excess is due to the photon-photon fusion, such a study seems possible even with $\sqrt{s} = 1$ TeV and $L = 1$ ab^{-1}.

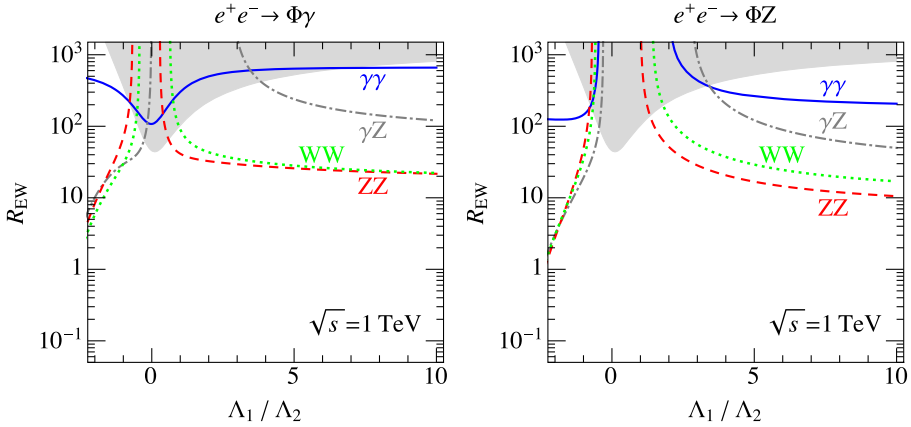

FIG. 7. The minimal values of $R_{\rm EW}$ to realize $S_{VV_1'V_2'}/\sqrt{B_{VV_1'V_2'}} > 5$ for $V_1'V_2' = \gamma\gamma$ (blue solid), γZ (gray dot-dashed), ZZ (red dashed), and W^+W^- (green dotted) as a function of the ratio Λ_1/Λ_2. Here we take $\sqrt{s} = 1$ TeV, $L = 1$ ab^{-1}, $P_{e-} = P_{e+} = 0$, and $\sigma_{\rm LHC}(pp \to \Phi \to \gamma\gamma) = 10$ fb. In the shaded region, $\sigma^{(\gamma\gamma)}_{\rm LHC}(pp \to \Phi \to \gamma\gamma)$ is larger than $\sigma^{(gg)}_{\rm LHC}(pp \to \Phi \to \gamma\gamma)$.

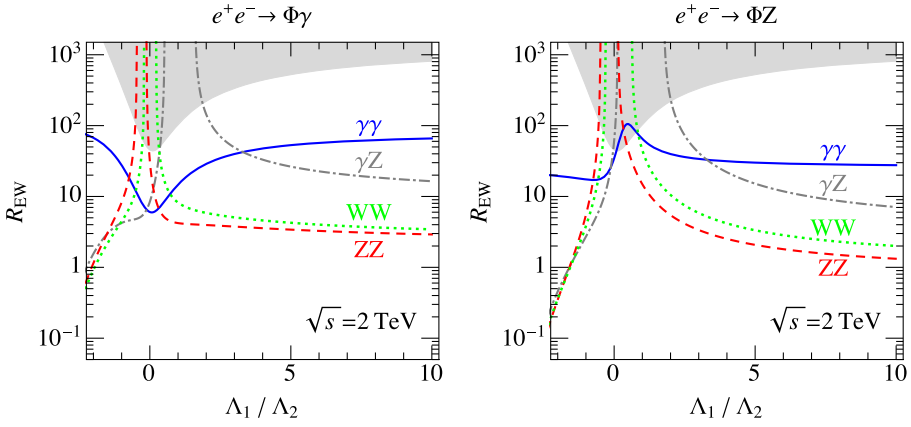

FIG. 8. Same as Fig. 7, except for $\sqrt{s} = 2$ TeV.

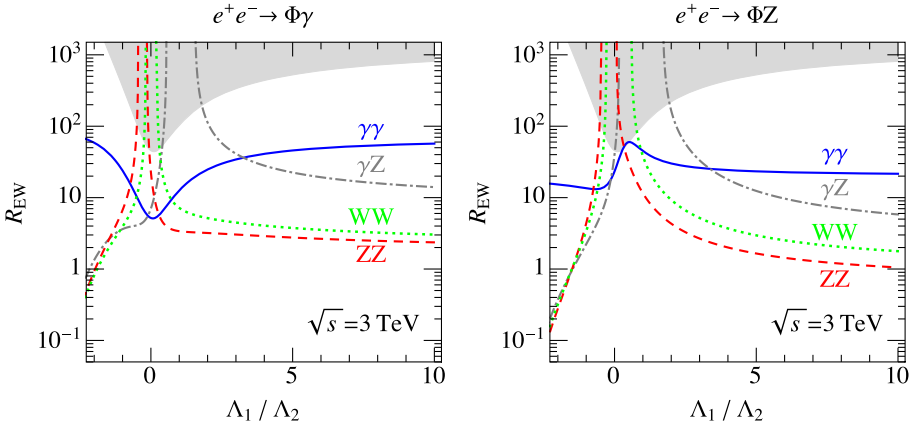

FIG. 9. Same as Fig. 7, except for $\sqrt{s} = 3$ TeV.

B. $e^+e^- \to e^+e^-\Phi$

Next, we consider the process $e^+e^- \to e^+e^-\Phi$. The important feature of such a process is the existence of $e^\pm$ which are (almost) parallel to the beam direction. Detection of such $e^\pm$ may help to reduce backgrounds.

We consider the case where at least one of the final-state $e^\pm$ is detectable. Then, as the signal, we require

(i) Requirement 1 in the previous section: At least one $e^\pm$ with $E_{e^\pm} > 50$ GeV and $\theta_{e^\pm} > 10$ mrad. In addition, $\theta_{e^\pm} < 100$ mrad for both e^+ and e^-.

(ii) Candidates of V_1' and V_2', which are the gauge bosons produced by the decay of Φ. [Thus, $(V_1', V_2') = (\gamma,\gamma), (g,g), (\gamma, Z), (Z, Z)$, or (W^+, W^-).]

In the following, we estimate the number of SM backgrounds for these types of events. In order to reduce the backgrounds, we impose kinematical selections based on the invariant mass of the $V_1'V_2'$ system (which is denoted as $m_{V_1'V_2'}$) and the pseudorapidities of V_1' and V_2' since some of the final-state gauge bosons are likely to be emitted to the forward direction:

(i) $|m_{V_1'V_2'} - m_\Phi| < 0.02 m_\Phi$ for $(V_1', V_2') = (\gamma,\gamma)$, and $|m_{V_1'V_2'} - m_\Phi| < 0.06 m_\Phi$ otherwise.

(ii) $|\eta| < 1.47$ for V_1' and V_2'.

Notice that, for the signal events with $\Phi \to gg$, we expect that the dominant background is the process $e^+e^- \to e^+e^-q\bar{q}$. Thus, we also study the cross section of such a process.

Now we estimate the number of SM backgrounds. If there exists the process $\gamma\gamma \to V_1'V_2'$, the cross section of $e^+e^- \to e^+e^-V_1'V_2'$ is logarithmically enhanced when the final-state e^+ and e^- are both emitted to the forward directions. This is because diagrams containing n nearly on-shell photon propagators result in the cross section approximately proportional to $\ln^n(|q^2|^{(\max)}/|q^2|^{(\min)})$, as we discussed in the previous section [see Eq. (3.5)].

We first consider the cases where the final states are $q\bar{q}$ or W^+W^-. In these cases, there exist tree-level processes $\gamma\gamma \to q\bar{q}$ and W^+W^-. Therefore, for the backgrounds of these signal processes, diagrams with two nearly on-shell photon propagators are expected to be the most important. By using the equivalent photon approximation, we estimate the SM cross sections of the processes $e^+e^- \to e^+e^-q\bar{q}$ and $e^+e^-W^+W^+$, imposing the above-mentioned kinematical selections. The expected numbers of backgrounds for $L = 1$ ab^{-1} are 47 and 530 for $(V_1', V_2') = (g, g)$ and (W^+, W^-), respectively, taking $\sqrt{s} = 1$ TeV. For $\sqrt{s} = 2$ TeV, they are 250 and 2500, and for $\sqrt{s} = 3$ TeV, 380 and 3700, respectively. Since signal events with these final states suffer from large numbers of backgrounds compared to the other final states, as we will see below, we will not discuss further the detectability of these signal events.

We now consider the signals with $\Phi \to V_1'V_2'$ with $(V_1', V_2') = (\gamma,\gamma), (\gamma, Z)$, and (Z, Z). For these final states, the processes $\gamma\gamma \to V_1'V_2'$ occur at the one-loop level, and are loop suppressed. Assuming that the one-loop processes with maximal logarithmic enhancements dominate the backgrounds, we estimate the number of backgrounds using the equivalent photon approximation; the cross sections of the processes $\gamma\gamma \to \gamma\gamma$, γZ, and ZZ can be found in [28–30]. Then, the numbers of backgrounds are estimated to be 0.2, 3.1, and 5.1 for $(V_1', V_2') = (\gamma,\gamma)$, (γ, Z), and (Z, Z), taking $L = 1$ ab^{-1} and $\sqrt{s} = 1$ TeV. For $\sqrt{s} = 2$ TeV (3 TeV), they are 1.0, 17, and 28 (1.5, 25, and 42), respectively.[3]

With these background estimations, we calculate the minimal value of $R_{\rm EW}$ which realizes $S_{eeV_1'V_2'}/\sqrt{B_{eeV_1'V_2'}} > 5$ for $L = 1$ ab^{-1}, where

$$S_{eeV_1'V_2'} \equiv L\sigma(e^+e^- \to e^+e^-\Phi)\mathrm{Br}(\Phi \to V_1'V_2')\epsilon, \quad (4.5)$$

while $B_{eeV_1'V_2'}$ is the number of backgrounds. If $B_{eeV_1'V_2'}$ is less than 1, we require $S_{eeV_1'V_2'} > 5$ instead. In Figs. 10, 11,

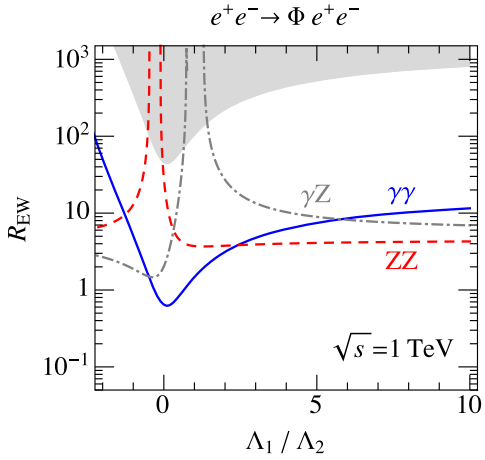

FIG. 10. The minimal values of $R_{\rm EW}$ to realize $S_{VV_1'V_2'}/\sqrt{B_{VV_1'V_2'}} > 5$ for $V_1'V_2' = \gamma\gamma$ (blue solid), γZ (gray dot-dashed), and ZZ (red dashed) as functions of the ratio Λ_1/Λ_2. In the shaded region, $\sigma^{(\gamma\gamma)}_{\rm LHC}(pp \to \Phi \to \gamma\gamma)$ is larger than $\sigma^{(gg)}_{\rm LHC}(pp \to \Phi \to \gamma\gamma)$. Here we take $\sqrt{s} = 1$ TeV, $L = 1$ ab^{-1}, and $P_{e-} = P_{e+} = 0$.

[3] In the tree-level diagrams contributing to the backgrounds of these processes, the number of nearly on-shell photon propagator is at most one. However, the tree-level contributions are potentially important because there is no loop suppression. We have also studied the tree-level contributions by using `MadGraph5_aMC@NLO v2` [31] and `MadAnalysis` [32]. For $10 < \theta_{e^\pm} < 100$ mrad for both e^+ and e^-, we directly calculated the cross section of the process $e^+e^- \to e^+e^-V_1'V_2'$. For $\theta_{e^+} < 10$ mrad and $10 < \theta_{e^-} < 100$ mrad, (or for $\theta_{e^-} < 10$ mrad and $10 < \theta_{e^+} < 100$ mrad), we adopted the equivalent photon approximation for the virtual photon emitted by e^+ (or e^-) and estimated the cross section. For both regions of the phase space, we found that the number of backgrounds with $L = 1$ ab are much smaller than 1. Thus, we neglect the tree-level contributions.

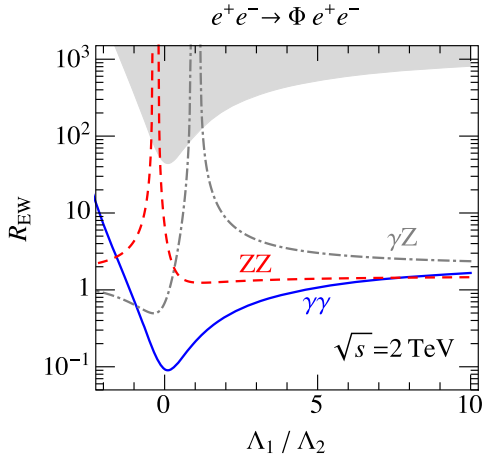

FIG. 11. Same as Fig. 10, except for $\sqrt{s} = 2$ TeV.

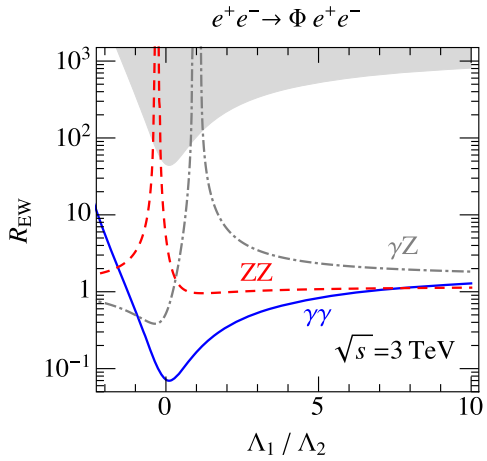

FIG. 12. Same as Fig. 10, except for $\sqrt{s} = 3$ TeV.

and 12, we show the minimal values of $R_{\rm EW}$ as functions of the ratio Λ_1/Λ_2, taking $\sqrt{s} = 1$, 2, and 3 TeV. Comparing with Figs. 7–9, we can see that the process $e^+e^- \to e^+e^-\Phi$ is easier to detect than $e^+e^- \to \Phi V$ if Φ decays into a pair of neutral electroweak gauge bosons.

V. INVISIBLE DECAY

In the previous section, we have considered the decay of Φ into SM gauge bosons. Notably, Φ may also couple to a new particle which is not in the particle content of the SM. In this section, we consider the case where Φ couples to a particle which does not have a direct coupling to SM particles. In such a case, Φ has an invisible decay mode; study of such a decay mode is an important step to understand the property of Φ.

One possibility of detecting the invisible decay of Φ at the e^+e^- colliders is to use the production process $e^+e^- \to \Phi\gamma$ and ΦZ, followed by the invisible decay of Φ. In such processes, we observe energetic γ or the decay products of Z accompanied by large missing momentum. In the signal event, the energy of the SM gauge boson is $E_V^{(\rm sig)}$ given in Eq. (4.1). Thus, by selecting events with a single γ or Z candidate whose energy is close enough to $E_V^{(\rm sig)}$, we may be able to eliminate backgrounds to observe the invisible decay of Φ.

For such a study, we estimate the number of backgrounds, applying cuts on the energy of SM gauge bosons. For the signal process $e^+e^- \to \Phi\gamma$ with $\Phi \to \chi\chi$, we expect a single photon final state. As possible sources of backgrounds, we consider the following processes:

(i) $e^+e^- \to \gamma\bar{\nu}_l\nu_l$,
(ii) $e^+e^- \to \gamma\bar{\nu}_l\nu_l\bar{\nu}_{l'}\nu_{l'}$,

with $l, l' = e$, μ, and τ; we calculate the cross sections of these processes requiring that the energy of γ is in the range of $|E_\gamma - E_\gamma^{(\rm sig)}| < 0.02E_\gamma^{(\rm sig)}$. We also require $|\eta| < 1$ for the final-state photon to optimize the detectability. For the signal process $e^+e^- \to \Phi Z$ with $\Phi \to \chi\chi$, monochromatic Z-boson should be tagged to identify the signal. Here, we use the hadronic decay of Z because the hadronic branching ratio is larger than leptonic one. Then, we estimate the number of backgrounds by calculating the cross sections of the following processes[4]:

(i) $e^+e^- \to Z\bar{\nu}_l\nu_l$,
(ii) $e^+e^- \to Z\bar{\nu}_l\nu_l\bar{\nu}_{l'}\nu_{l'}$,

where we require that $|E_Z - E_Z^{(\rm sig)}| < 0.06E_\gamma^{(\rm sig)}$, and that $|\eta| < 1$ for the Z-boson. We use `MadGraph5_aMC@NLO v2` [31] and `MadAnalysis` [32] to calculate the cross sections of the background processes. The numbers of backgrounds of these processes with the luminosity of 1ab^{-1} are summarized in Table V, taking $(P_{e^-}, P_{e^+}) = (+0.8, -0.3)$ and $(-0.8, +0.3)$. (We checked that one of these combinations of the helicities gives the best detectability, as far as $|P_{e^-}| = 0.8$ and $|P_{e^+}| = 0.3$.)

The detectability of the invisible decay mode is studied by calculating the following quantity:

$$S_{V\chi\chi}/\sqrt{B_{V\chi\chi}} \equiv \frac{L\sigma(e^+e^- \to \Phi V)\text{Br}(\Phi \to \chi\chi)\epsilon}{\sqrt{B_{V\chi\chi}}}, \quad (5.1)$$

where $B_{V\chi\chi}$ is the total number of the backgrounds for the process $e^+e^- \to \Phi V$ followed by the invisible decay of Φ. When the gluon-gluon fusion process dominates the LHC diphoton signal events, $S_{V\chi\chi}/\sqrt{B_{V\chi\chi}}$ is proportional to the ratio of $\Gamma(\Phi \to \chi\chi)/\Gamma(\Phi \to gg)$, as can be understood from Eq. (3.1). On the other hand, it is proportional $\Gamma(\Phi \to \chi\chi)/\Gamma(\Phi \to \gamma\gamma)$ for the case where the photon-photon

[4]Hadrons may be also produced by the scatterings of energetic photons emitted by the initial-state e^+ and e^- beams. However, in such events, the missing transverse momentum is expected to be small because the initial-state photons are expected to be (almost) parallel to the beam axis. Thus, we assume that such potential backgrounds can be eliminated by imposing a kinematical cut on the missing transverse momentum.

TABLE V. The number of backgrounds for $e^+e^- \to \Phi\gamma$ and ΦZ followed by $\Phi \to \chi\chi$, with $\sqrt{s} = 1$ and 2 TeV, and $L = 1$ ab^{-1}. Here we take $P_{e^-} = +0.8(-0.8)$ and $P_{e^+} = -0.3(+0.3)$ for the left (right) of each column.

	$\gamma + 2\nu$	$\gamma + 4\nu$	$Z + 2\nu$	$Z + 4\nu$
$\sqrt{s} = 1$ TeV	560 (9100)	3.6 (37)	4800 (80000)	22 (330)
$\sqrt{s} = 2$ TeV	78 (1100)	1.9 (9.3)	390 (6000)	5.1 (35)
$\sqrt{s} = 3$ TeV	32 (410)	1.6 (5.2)	130 (1800)	3.4 (14)

fusion process is the origin of the LHC diphoton excess [see Eq. (3.2)]. We have estimated the minimal values of these ratios as functions of Λ_1/Λ_2 to observe the invisible decay of Φ at the level of $S_{V\chi\chi}/\sqrt{B_{V\chi\chi}} > 5$. The results are shown in Figs. 13 and 14 for $e^+e^- \to \Phi\gamma$ and ΦZ, respectively. For the case where the diphoton excess at the LHC originates from the gluon-gluon fusion process, for example, the ILC with $\sqrt{s} = 1$ TeV and $L = 1$ ab^{-1} may observe the invisible decay of Φ when $\Gamma(\Phi \to \chi\chi)/\Gamma(\Phi \to gg) \sim O(10)$. Furthermore, the sensitivity depends on the beam polarizations. To see this, in Figs. 15 and 16,

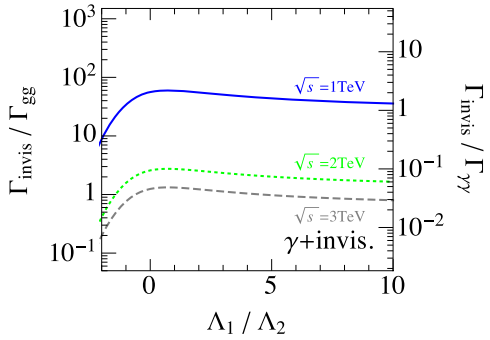

FIG. 13. The minimal values of $\Gamma(\Phi \to \chi\chi)/\Gamma(\Phi \to gg)$ (left horizontal axis, for the case where the LHC diphoton excess is due to the gluon-gluon fusion) and $\Gamma(\Phi \to \chi\chi)/\Gamma(\Phi \to \gamma\gamma)$ (right-horizontal axis, for the case where the LHC diphoton excess is due to the photon-photon fusion) to realize $S_{\gamma\chi\chi}/\sqrt{B_{\gamma\chi\chi}} > 5$, using the production process of $e^+e^- \to \Phi\gamma$. Here, we take $\sqrt{s} = 1$ TeV (blue solid), 2 TeV (green dotted), 3 TeV (gray dashed), and $L = 1$ ab^{-1}. In addition, the helicities of $e^\pm$ are $P_{e^-} = P_{e^+} = 0$.

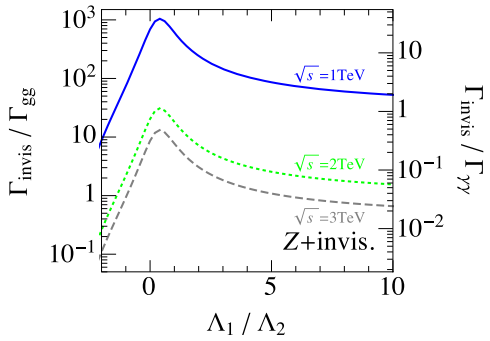

FIG. 14. Same as Fig. 13, except for $e^+e^- \to \Phi Z$.

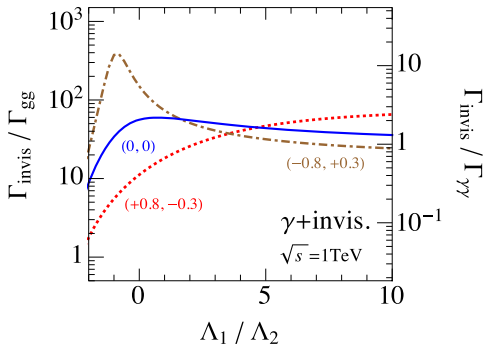

FIG. 15. The minimal values of $\Gamma(\Phi \to \chi\chi)/\Gamma(\Phi \to gg)$ (left horizontal axis, for the case where the LHC diphoton excess is due to the gluon-gluon fusion) and $\Gamma(\Phi \to \chi\chi)/\Gamma(\Phi \to \gamma\gamma)$ (right-horizontal axis, for the case where the LHC diphoton excess is due to the photon-photon fusion) to realize $S_{\gamma\chi\chi}/\sqrt{B_{\gamma\chi\chi}} > 5$, using the production process of $e^+e^- \to \Phi\gamma$. Here, we take $\sqrt{s} = 1$ TeV, and $L = 1$ ab^{-1}. In addition, the helicities of $e^\pm$ are $(P_{e-}, P_{e+}) = (+0.8, -0.3)$ (red dashed), $(-0.8, +0.3)$ (brown dot-dashed), and (0,0) (blue solid).

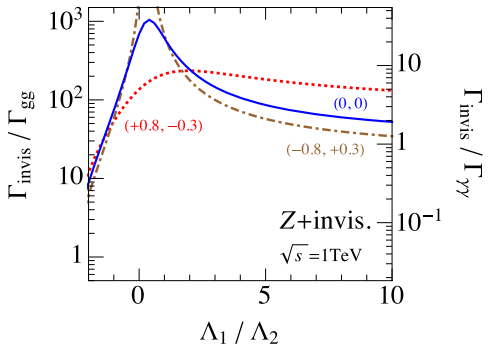

FIG. 16. Same as Fig. 13, except for $e^+e^- \to \Phi Z$.

we show the expected sensitivity with different beam polarizations for $\sqrt{s} = 1$ TeV.

VI. CONCLUSIONS AND DISCUSSION

In this paper, we have studied the prospect of investigating the scalar boson Φ, which is responsible for the diphoton excess observed at the LHC, using the future e^+e^- colliders. We have concentrated on the case where the LHC diphoton excess originates from the gluon-gluon and/or photon-photon fusion processes. We assumed that there exists a scalar boson Φ with its mass of ~750 GeV, and that Φ directly couples to the SM gauge bosons via the dimension-five operators [see Eq. (2.1)].

We have studied the production process of Φ in association with a SM gauge boson (i.e., γ or Z) and the production via the vector-boson fusion. We have calculated the cross sections of these processes. Then we have investigated the detectability of Φ with estimating the SM backgrounds. Detection of the decay mode of Φ into the gluon pair seems difficult because the number of backgrounds is large. With

the vector-boson fusion process, the decay of Φ into the electroweak gauge bosons may be detected at the e^+e^- colliders if the decay width of such processes are of the same order of $\Gamma(\Phi \to gg)$, assuming that the LHC diphoton excess is due to the gluon-gluon fusion. In order to observe Φ, the detection of energetic $e^\pm$ in the forward directions is crucial to eliminate the backgrounds. We found that the observations of the associated production with γ or Z are more difficult because the numbers of backgrounds are order of magnitude larger. We have also studied the possibility of detecting the invisible decay of Φ using the production process in association with γ or Z.

We comment on another possibility to study Φ at the future e^+e^- facilities. Because Φ couples directly to the photon pair, it can be produced at the photon-photon collider which is an important option of the future e^+e^- facilities. Indeed, in [20], it was shown that, even if the LHC diphoton excess originates from the gluon-gluon fusion, the Φ production cross section at the photon-photon collider can be as large as $\sim$100 fb for $\sqrt{s} \sim 1$ TeV, which is much larger than that with the e^+e^- collision. With such a large cross section, a significant number of Φ will be available for its detailed study.

Based on our analysis, the expected number of Φ production at the ILC is of $O(10)$ with $\sqrt{s} = 1$ TeV and $L = 1$ ab^{-1}, if the LHC diphoton excess is due to the gluon-gluon fusion and also if Φ dominantly decays into the gluon pair. If the LHC diphoton excess is from the photon-photon fusion, the number of Φ produced at the ILC becomes larger. In addition, even if the Φ production at the LHC is dominated by the gluon-gluon fusion, the invisible decay of Φ may be observed at the ILC if the invisible decay width is an order of magnitude larger than the decay width into the gluon pair. Thus, the ILC will provide interesting possibilities to study the properties of the diphoton resonance.

ACKNOWLEDGMENTS

The authors are grateful to Y. Takaesu for the collaboration at the early stage of this project. They also thank K. Fujii and T. Tanabe for useful comments. The work of T. M. is supported by JSPS KAKENHI No. 26400239. The authors thank K. Fujii for pointing this out.

APPENDIX: CROSS SECTIONS

In this Appendix, we give the expressions for the cross sections of the resonance production in association with SM gauge bosons. For the case with pseudoscalar resonance, we adopt the interaction terms given in Eq. (2.1). For completeness, we also consider the case where the new scalar resonance is a scalar boson, for which the interaction terms are given by[5]

$$\mathcal{L}_{\rm eff} = \frac{1}{\Lambda_1}\Phi\mathcal{B}_{\mu\nu}\mathcal{B}^{\mu\nu} + \frac{1}{\Lambda_2}\Phi\mathcal{W}^a_{\mu\nu}\mathcal{W}^{a\mu\nu} + \frac{1}{\Lambda_3}\Phi\mathcal{G}^A_{\mu\nu}\mathcal{G}^{A\mu\nu}. \tag{A1}$$

The following formulas can be used for both pseudoscalar and scalar cases.

Then, denoting the angle between the beam axis and the direction of the Φ in the CM frame as θ, the differential cross sections of the Φ production in association with a SM gauge boson with fully polarized initial state $e^\pm$ is given by

$$\frac{d\sigma(e^+_R e^-_L \to \Phi V)}{d\cos\theta} = \frac{\beta}{32\pi} C_V^{(L)} [s^2\beta^2(1+\cos^2\theta) + 8\xi_\Phi s m_V^2], \tag{A2}$$

with $V = \gamma$ and Z; $d\sigma(e^+_L e^-_R \to \Phi V)/d\cos\theta$ can be obtained by exchanging $L \leftrightarrow R$, while $\sigma(e^+_L e^-_L \to \Phi V) = \sigma(e^+_R e^-_R \to \Phi V) = 0$. Here, $\xi_\Phi = 0$ for the pseudoscalar production processes, while $\xi_\Phi = 1$ for the scalar production, $m_V = 0$ and m_Z for $V = \gamma$ and Z, respectively, and

$$\beta = \frac{1}{s}\sqrt{s^2 - 2(m_\Phi^2 + m_V^2)s + (m_\Phi^2 - m_V^2)^2}. \tag{A3}$$

In addition,

$$C_\gamma^{(L,R)} = \left[\frac{2e}{\Lambda_{\gamma\gamma}s} - \frac{g_{Ze}^{(L,R)}}{\Lambda_{\gamma Z}(s-m_Z^2)}\right]^2, \tag{A4}$$

$$C_Z^{(L,R)} = \left[\frac{e}{\Lambda_{\gamma Z}s} - \frac{2g_{Ze}^{(L,R)}}{\Lambda_{ZZ}(s-m_Z^2)}\right]^2, \tag{A5}$$

where

$$\Lambda_{\gamma\gamma}^{-1} \equiv \frac{g_1^2}{g_Z^2}\Lambda_2^{-1} + \frac{g_2^2}{g_Z^2}\Lambda_1^{-1}, \tag{A6}$$

$$\Lambda_{\gamma Z}^{-1} \equiv \frac{2g_1g_2}{g_Z^2}(\Lambda_2^{-1} - \Lambda_1^{-1}), \tag{A7}$$

$$\Lambda_{ZZ}^{-1} \equiv \frac{g_2^2}{g_Z^2}\Lambda_2^{-1} + \frac{g_1^2}{g_Z^2}\Lambda_1^{-1}, \tag{A8}$$

with g_1 and g_2 being the gauge coupling constants of $U(1)_Y$ and $SU(2)_L$, respectively, $g_Z \equiv \sqrt{g_1^2 + g_2^2}$,[6] and

$$e = \frac{g_1g_2}{g_Z}, \qquad g_{Ze}^{(L)} = \frac{g_1^2 - g_2^2}{2g_Z}, \qquad g_{Ze}^{(R)} = \frac{g_1^2}{g_Z}. \tag{A9}$$

[5]For the notational simplicity, we use the same notation for the suppression scales of the dimension-five operators in the pseudoscalar and scalar cases.

[6]In our numerical calculations, we use the gauge coupling constants at the renormalization scale of $\mu = m_Z$. For more accurate calculations, inclusion of the effects of renormalization group running of the gauge coupling constants are relevant.

[1] T. Behnke *et al.*, The international linear collider technical design report, volume 1: Executive summary, arXiv:1306.6327.
[2] H. Baer *et al.*, The international linear collider technical design report, volume 2: Physics, arXiv:1306.6352.
[3] C. Adolphsen *et al.*, The international linear collider technical design report, volume 3.I: Accelerator & in the technical design phase, arXiv:1306.6353.
[4] C. Adolphsen *et al.*, The international linear collider technical design report, volume 3.II: Accelerator baseline design, arXiv:1306.6328.
[5] T. Behnke *et al.*, The international linear collider technical design report, volume 4: Detectors, arXiv:1306.6329.
[6] L. Linssen, A. Miyamoto, M. Stanitzki, and H. Weerts, Physics and detectors at CLIC: CLIC conceptual design report, arXiv:1202.5940.
[7] ATLAS Collaboration, Report No. ATLAS-CONF-2015-081, 2015.
[8] CMS Collaboration, Report No. CMS PAS EXO-15-004, 2015.
[9] K. Harigaya and Y. Nomura, Composite models for the 750 GeV diphoton excess, Phys. Lett. B **754**, 151 (2016).
[10] Y. Mambrini, G. Arcadi, and A. Djouadi, The LHC diphoton resonance and dark matter, Phys. Lett. B **755**, 426 (2016).
[11] M. Backovic, A. Mariotti, and D. Redigolo, Di-photon excess illuminates dark matter, J. High Energy Phys. 03 (2016) 157.
[12] A. Angelescu, A. Djouadi, and G. Moreau, Scenarii for interpretations of the LHC diphoton excess: two Higgs doublets and vector-like quarks and leptons, Phys. Lett. B **756**, 126 (2016).
[13] Y. Nakai, R. Sato, and K. Tobioka, Footprints of New Strong Dynamics via Anomaly, Phys. Rev. Lett. **116**, 151802 (2016).
[14] S. Knapen, T. Melia, M. Papucci, and K. Zurek, Rays of light from the LHC, Phys. Rev. D **93**, 075020 (2016).
[15] D. Buttazzo, A. Greljo, and D. Marzocca, Knocking on new physics door with a scalar resonance, Eur. Phys. J. C **76**, 116 (2016).
[16] A. Pilaftsis, Diphoton signatures from heavy axion decays at the CERN Large Hadron Collider, Phys. Rev. D **93**, 015017 (2016).
[17] R. Franceschini, G. F. Giudice, J. F. Kamenik, M. McCullough, A. Pomarol, R. Rattazzi, M. Redi, F. Riva, A. Strumia, and R. Torre, What is the $\gamma\gamma$ resonance at 750 GeV?, J. High Energy Phys. 03 (2016) 144.
[18] S. Di Chiara, L. Marzola, and M. Raidal, First interpretation of the 750 GeV di-photon resonance at the LHC, Phys. Rev. D **93**, 095018 (2016).
[19] T. Higaki, K. S. Jeong, N. Kitajima, and F. Takahashi, The QCD axion from aligned axions and diphoton excess, Phys. Lett. B **755**, 13 (2016).
[20] H. Ito, T. Moroi, and Y. Takaesu, Studying 750 GeV diphoton resonance at photon-photon collider, Phys. Lett. B **756**, 147 (2016).
[21] N. Sonmez, Charged Higgs pair production in THDM through photon-photon collisions at the ILC, arXiv:1601.01837.
[22] A. Djouadi, J. Ellis, R. Godbole, and J. Quevillon, Future collider signatures of the possible 750 GeV state, J. High Energy Phys. 03 (2016) 205.
[23] M. He, X. G. He, and Y. Tang, A $\gamma\gamma$ Collider for the 750 GeV resonant state, Phys. Lett. B **759**, 166 (2016).
[24] C. Csaki, J. Hubisz, and J. Terning, Minimal model of a diphoton resonance: Production without gluon couplings, Phys. Rev. D **93**, 035002 (2016).
[25] C. Csaki, J. Hubisz, S. Lombardo, and J. Terning, Gluon versus photon production of a 750 GeV diphoton resonance, Phys. Rev. D **93**, 095020 (2016).
[26] G. Aad *et al.* (ATLAS Collaboration), Search for new resonances in $W\gamma$ and $Z\gamma$ final states in pp collisions at $\sqrt{s} = 8$ TeV with the ATLAS detector, Phys. Lett. B **738**, 428 (2014).
[27] V. M. Budnev, I. F. Ginzburg, G. V. Meledin, and V. G. Serbo, The two photon particle production mechanism. Physical problems. Applications. Equivalent photon approximation, Phys. Rep. **15**, 181 (1975).
[28] G. J. Gounaris, P. I. Porfyriadis, and F. M. Renard, The $\gamma\gamma \to \gamma\gamma$ process in the standard and SUSY models at high energies, Eur. Phys. J. C **9**, 673 (1999).
[29] G. J. Gounaris, J. Layssac, P. I. Porfyriadis, and F. M. Renard, The $\gamma\gamma \to \gamma Z$ process at high-energies and the search for virtual SUSY effects, Eur. Phys. J. C **10**, 499 (1999).
[30] G. J. Gounaris, J. Layssac, P. I. Porfyriadis, and F. M. Renard, The $\gamma\gamma \to ZZ$ process and the search for virtual SUSY effects at a $\gamma\gamma$ collider, Eur. Phys. J. C **13**, 79 (2000).
[31] J. Alwall, R. Frederix, S. Frixione, V. Hirschi, F. Maltoni, O. Mattelaer, H.-S. Shao, T. Stelzer, P. Torrielli, and M. Zaro, The automated computation of tree-level and next-to-leading order differential cross sections, and their matching to parton shower simulations, J. High Energy Phys. 07 (2014) 079.
[32] E. Conte, B. Fuks, and G. Serret, MadAnalysis 5, a user-friendly framework for collider phenomenology, Comput. Phys. Commun. **184**, 222 (2013).